Electronic Supplementary Material (ESI) for Soft Matter.
This journal is © The Royal Society of Chemistry 2023

Supplementary Information to Reaction-Driven Assembly: Controlling Changes in Membrane Topology by Reaction Cycles

Gregor Häfner[ab], Marcus Müller*[a]

1 Chemical Potentials and Time Evolution in the UDM

Starting from the free-energy functional of the equilibrium Uneyama-Doi model (UDM), we derive the explicit form of the chemical potentials for the model system of a diblock copolymer P (amphiphilic product), consisting of blocks A, B, and a homopolymer R (hydrophilic reactant) in solution S/F. Taking Equation 3 and the definition $\mu_c(\mathbf{r}) = \delta\mathscr{F}/\delta\phi(\mathbf{r})$, one obtains

$$\frac{\mu_A(\mathbf{r})R_\mathrm{e}^3}{\sqrt{\bar{\mathscr{N}}}k_\mathrm{B}T} = \frac{18}{R_\mathrm{e}^2 f_A f_B}\frac{1}{\psi_A}\int \mathrm{d}\mathbf{r}'\,\mathscr{G}(\mathbf{r}-\mathbf{r}')\left[f_B\psi_A(\mathbf{r}') - \sqrt{f_A f_B}\psi_B(\mathbf{r}')\right] + \frac{\tilde{s}(f_A)}{f_B}(2\ln\psi_A+1) - \frac{1}{2\sqrt{f_A f_B}}\frac{\psi_B}{\psi_A} - \frac{R_\mathrm{e}^2}{6}\frac{\nabla^2\psi_A}{\psi_A} + \sum_{c\neq A}\chi_{Ac}N_P\psi_c^2 + \pi N_P \tag{SI.1}$$

$$\frac{\mu_B(\mathbf{r})R_\mathrm{e}^3}{\sqrt{\bar{\mathscr{N}}}k_\mathrm{B}T} = \frac{18}{R_\mathrm{e}^2 f_A f_B}\frac{1}{\psi_B}\int \mathrm{d}\mathbf{r}'\,\mathscr{G}(\mathbf{r}-\mathbf{r}')\left[f_A\psi_B(\mathbf{r}') - \sqrt{f_A f_B}\psi_A(\mathbf{r}')\right] + \frac{\tilde{s}(f_B)}{f_A}(2\ln\psi_B+1) - \frac{1}{2\sqrt{f_A f_B}}\frac{\psi_A}{\psi_B} - \frac{R_\mathrm{e}^2}{6}\frac{\nabla^2\psi_B}{\psi_B} + \sum_{c\neq B}\chi_{Bc}N_P\psi_c^2 + \pi N_P \tag{SI.2}$$

$$\frac{\mu_{\tilde{c}}(\mathbf{r})R_\mathrm{e}^3}{\sqrt{\bar{\mathscr{N}}}k_\mathrm{B}T} = \frac{N_P}{N_{\tilde{c}}}(2\ln\psi_{\tilde{c}}+1) - \frac{R_\mathrm{e}^2}{6}\frac{\nabla^2\psi_{\tilde{c}}}{\psi_{\tilde{c}}} + \sum_{c\neq\tilde{c}}\chi_{\tilde{c}c}N_P\psi_c^2 + \pi N_P \tag{SI.3}$$

for $\tilde{c} = S,F,R$ and the definition $\psi_c(\mathbf{r}) = \sqrt{\phi_c(\mathbf{r})}$. Using these chemical potentials in the model-B dynamics and including the reaction terms, we obtain the full set of governing evolution equations

$$\partial_t\phi_A(\mathbf{r},t) = \frac{\lambda R_\mathrm{e}^5}{\sqrt{\bar{\mathscr{N}}}k_\mathrm{B}T}\nabla\cdot[\phi_A\nabla\mu_A] + \xi_A + f_A r_f N_P\phi_F\phi_R - r_b N_P\phi_A \tag{SI.4}$$

$$\partial_t\phi_B(\mathbf{r},t) = \frac{\lambda R_\mathrm{e}^5}{\sqrt{\bar{\mathscr{N}}}k_\mathrm{B}T}\nabla\cdot[\phi_B\nabla\mu_B] + \xi_B + f_B r_f N_P\phi_F\phi_R - r_b N_P\phi_B \tag{SI.5}$$

$$\partial_t\phi_R(\mathbf{r},t) = \frac{\lambda R_\mathrm{e}^5}{\sqrt{\bar{\mathscr{N}}}k_\mathrm{B}T}\nabla\cdot[\phi_R\nabla\mu_R] + \xi_R - r_f N_P\phi_F\phi_R + r_b N_P(\phi_A+\phi_B) \tag{SI.6}$$

$$\partial_t\phi_{S/F}(\mathbf{r},t) = \frac{\lambda R_\mathrm{e}^5}{\sqrt{\bar{\mathscr{N}}}k_\mathrm{B}T}\nabla\cdot\left[\phi_{S/F}\nabla\mu_{S/F}\right] + \xi_{S/F} \tag{SI.7}$$

where the fuel F is not consumed in the forward reaction.

2 Growth Rates of Phase-Separation Processes

To calculate the growth rates for the phase separation processes between diblock copolymer (amphiphile) and solvent as well as between the two blocks of the copolymer, we perform a linear stability analysis of the time evolution around a spatially homogeneous concentration. We invoke the two simplifications in Analytical Predictions of the main text: (i) We assume the fuel be homogeneously distributed, $\phi_F(\mathbf{r}) = \rho_F$. (ii) Moreover, we assume $\phi_R(\mathbf{r})/\rho_R = \phi_S(\mathbf{r})/\rho_S$ and introduce

[a] *Institute for Theoretical Physics, Georg-August University, Friedrich-Hund-Platz 1, 37077 Göttingen, Germany. E-mail: mmueller@theorie.physik.uni-goettingen.de*
[b] *Max Planck School Matter to Life, Jahnstraße 29, 69120 Heidelberg, Germany*

a joint density for the hydrophilic components, $\phi_H = \phi_S + \phi_R$, and concomitant chemical potential

$$\begin{aligned}\frac{\mu_H(\mathbf{r})R_\mathrm{e}^3}{\sqrt{\mathscr{N}}k_\mathrm{B}T} &= \frac{\rho_S}{\rho_H}\frac{N_P}{N_S}(2\ln\psi_S+1)+\frac{\rho_R}{\rho_H}\frac{N_P}{N_R}(2\ln\psi_R+1)\\ &\quad -\frac{R_\mathrm{e}^2}{6}\left(\frac{\rho_S}{\rho_H}\frac{\nabla^2\psi_S}{\psi_S}+\frac{\rho_R}{\rho_H}\frac{\nabla^2\psi_R}{\psi_R}\right)\\ &\quad +\chi_{AH}N_P\psi_A^2+\chi_{BH}N_P\psi_B^2+\pi N_P \qquad \text{(SI.8)}\\ &= \left(\frac{N_P}{N_S}\frac{\rho_S}{\rho_H}\ln\frac{\rho_S}{\rho_H}+\frac{N_P}{N_R}\frac{\rho_R}{\rho_H}\ln\frac{\rho_R}{\rho_H}\right)+\left(\frac{N_P}{N_S}\frac{\rho_S}{\rho_H}+\frac{N_P}{N_R}\frac{\rho_R}{\rho_H}\right)(\ln\psi_H^2+1)\\ &\quad -\frac{R_\mathrm{e}^2}{6}\frac{\nabla^2\psi_H}{\psi_H}+\chi_{AH}N_P\psi_A^2+\chi_{BH}N_P\psi_B^2+\pi N_P \qquad \text{(SI.9)}\end{aligned}$$

The incompressibility constraint, $\sum_c \phi_c(\mathbf{r}) = 1$, allows us to determine the Lagrange field, $\pi(\mathbf{r})$,[50] from the time evolution, Equation SI.4-SI.7, resulting in

$$\begin{aligned}\frac{\partial\phi_c}{\partial t} &= \nabla\cdot\left[\frac{\Lambda_c}{\sum_{c'}\Lambda_{c'}}\sum_{c'\neq c}(\Lambda_{c'}\nabla(\mu_c-\mu_{c'}))\right]+\frac{\mathrm{d}\phi_c^\mathrm{conv}}{\mathrm{d}t} \qquad \text{(SI.10)}\\ &= \frac{\lambda R_\mathrm{e}^5}{\sqrt{\mathscr{N}}k_\mathrm{B}T}\nabla\cdot\left[\sum_{c'\neq c}(\phi_c\phi_{c'}\nabla(\mu_c-\mu_{c'}))\right]+\frac{\mathrm{d}\phi_c^\mathrm{conv}}{\mathrm{d}t} \qquad \text{(SI.11)}\end{aligned}$$

where noise is ignored and in the second line the explicit form of the Onsager coefficient was used. Using $\phi_H = 1-\rho_F-\phi_A-\phi_B$, one is left with a time evolution for components A and B. Explicitly, we have

$$\partial_t\phi_A = \frac{\lambda R_\mathrm{e}^5}{\sqrt{\mathscr{N}}k_\mathrm{B}T}\nabla\cdot[\phi_A\phi_B\nabla(\mu_A-\mu_B)+\phi_A\phi_H\nabla(\mu_A-\mu_H)]+\frac{f_A r_f N_P\rho_F\rho_R}{\rho_H}\phi_H - r_b N_P\phi_A \qquad \text{(SI.12)}$$

$$\partial_t\phi_B = \frac{\lambda R_\mathrm{e}^5}{\sqrt{\mathscr{N}}k_\mathrm{B}T}\nabla\cdot[\phi_B\phi_A\nabla(\mu_B-\mu_A)+\phi_B\phi_H\nabla(\mu_B-\mu_H)]+\frac{f_B r_f N_P\rho_F\rho_R}{\rho_H}\phi_H - r_b N_P\phi_B \qquad \text{(SI.13)}$$

We linearize Equation SI.12 and SI.13 around the mean concentrations, $\phi_c(\mathbf{r},t) = \rho_c + \delta\phi_c(\mathbf{r},t)$ for small deviations $\delta\phi_c(\mathbf{r},t) \ll 1$. Defining $\boldsymbol{\delta\phi}(\mathbf{r},t) = (\delta\phi_A(\mathbf{r},t),\delta\phi_B(\mathbf{r},t))^\intercal$, we obtain

$$\partial_t\boldsymbol{\delta\phi}(\mathbf{r},t) = \Sigma[\nabla^2]\boldsymbol{\delta\phi}(\mathbf{r},t) \qquad \text{(SI.14)}$$

with the linear evolution operator $\Sigma[\nabla^2]$. This is readily solved in Fourier space where the equation becomes

$$\partial_t\hat{\boldsymbol{\delta\phi}}(\mathbf{q},t) = \hat{\Sigma}(\mathbf{q})\hat{\boldsymbol{\delta\phi}}(\mathbf{q},t), \qquad \text{(SI.15)}$$

yielding

$$\hat{\boldsymbol{\delta\phi}}(\mathbf{q},t) = c_+\hat{\boldsymbol{\delta\phi}}_+(\mathbf{q})e^{\sigma_+(\mathbf{q})t}+c_-\hat{\boldsymbol{\delta\phi}}_-(\mathbf{q})e^{\sigma_-(\mathbf{q})t} \qquad \text{(SI.16)}$$

$\boldsymbol{\delta\phi}_\pm(\mathbf{q})$ are the eigenvectors of the evolution operator, $\hat{\Sigma}(\mathbf{q})$, corresponding to the eigenvalues $\sigma_\pm(\mathbf{q})$, and $c_\pm \in \mathbb{R}$. The matrix elements of the Fourier-transformed evolution operator read

$$\hat{\Sigma}_{A,A}(\mathbf{q})/\lambda = \left[-\frac{9}{f_A} - \frac{r_b N_P}{\lambda}\left(\frac{\rho_A}{\rho_H}+1\right)\right] + \left[-\tilde{s}(f_A)\left(\rho_P + \frac{\rho_H}{f_B}\right) - \frac{1}{4f_A} - \rho_A\left(\frac{\rho_S N_P}{\rho_H N_S} + \frac{\rho_R N_P}{\rho_H N_R}\right) + \rho_A\rho_B(\chi_{AH} - \chi_{BH} + \chi_{AB})N_P + 2\rho_A\rho_H\chi_{AH}N_P\right](\mathbf{q}R_\mathrm{e})^2 - \frac{1}{12}(\mathbf{q}R_\mathrm{e})^4 \tag{SI.17}$$

$$\hat{\Sigma}_{A,B}(\mathbf{q})/\lambda = \left[\frac{9}{f_B} - \frac{r_b N_P \rho_A}{\lambda\rho_H}\right] + \left[\tilde{s}(f_B)\rho_P + \frac{1}{4f_B} - \rho_A\left(\frac{\rho_S N_P}{\rho_H N_S} + \frac{\rho_R N_P}{\rho_H N_R}\right) + \rho_A\rho_B(\chi_{AH} - \chi_{BH} - \chi_{AB})N_P + \rho_A\rho_H(\chi_{AH} + \chi_{BH} - \chi_{AB})N_P\right](\mathbf{q}R_\mathrm{e})^2 \tag{SI.18}$$

where we used $\rho_P = \rho_A + \rho_B$. The other entries, $\hat{\Sigma}_{B,A/B}(\mathbf{q})$, are obtained by exchanging $A \leftrightarrow B$. The evolution only depends on the absolute value of the wavevector, $q = |\mathbf{q}|$. The eigenvalues of the 2×2-matrix $\hat{\Sigma}(q)$ are given by the solution of the characteristic polynomial.

$$\sigma_\pm(q) = \frac{\mathrm{tr}(\hat{\Sigma}(q))}{2} \pm \sqrt{\frac{\mathrm{tr}(\hat{\Sigma}(q))^2}{4} - \det(\hat{\Sigma}(q))} \tag{SI.19}$$

In the simplest, most intuitive form, the two eigenvectors correspond to the two processes: "*PH*" – phase separation of polymer and solvent or "*AB*" – phase separation between the two polymer blocks, respectively. To illustrate this, it turns out to be useful to plot the angle of the corresponding (normalized) eigenvectors $\varphi_\pm(q) = \arctan2(\hat{\boldsymbol{\delta\phi}}_\pm(q)) \bmod \pi$. This quantity can be better understood by considering special cases (i) $\varphi = 0 \Rightarrow \delta\phi_A \neq 0, \delta\phi_B = 0$: *A* phase separates from *H*, (ii) $\varphi = \arctan(f_B/f_A) =: \varphi^* \Rightarrow \delta\phi_A/f_A = \delta\phi_B/f_B$: *A* and *B* phase separate from *H* (process *PH*), (iii) $\varphi = \frac{\pi}{2} \Rightarrow \delta\phi_A = 0$, $\delta\phi_B \neq 0$: *B* phase separates from *H* and (iv) $\varphi = \frac{3\pi}{4} \Rightarrow \delta\phi_A = -\delta\phi_B \Rightarrow \delta\phi_H = 0$: *A* phase separates from *B* (process *AB*).

First, we consider symmetric diblock copolymers (amphiphiles) in a nonselective solvent. The corresponding growth rates and angles of the eigenvectors are shown in Figure SI.1. Due to the symmetry, the two processes, $\Delta\phi_{AB}$ and $\Delta\phi_{PH}$, are eigenmodes of the linearized evolution operator for all wavevectors, q. However, the assignment to the eigenmodes switches, *i. e.*, for small qR_e the *PH* process corresponds to the fastest growing mode, $\Delta\phi_{PH} = \Delta\phi_+$, whereas for larger qR_e, microphase separation between *A* and *B* is the fastest growing mode. This switching occurs when the growth rates as a function of q cross.

The linear growth becomes more complicated for asymmetric diblock copolymers, as also shown in Figure SI.1: (i) The two processes of phase separation, macrophase separation *PH* and microphase separation *AB*, are no longer eigenmodes of the linearized evolution operator. (ii) The growth eigenmodes do not abruptly switch their process character but the angles $\varphi_\pm$ rather gradually change with wavevector, q. Moreover, the crossing of the growth rates $\sigma_\pm(q)$ is avoided.

Nevertheless, we can reveal the contribution of each process by projecting onto these. For this, we initialize the system,

$$\boldsymbol{\delta\phi}(q, t=0) = \boldsymbol{\delta\phi}_m = c_{+,m}(q)\hat{\boldsymbol{\delta\phi}}_+(q) + c_{-,m}(q)\hat{\boldsymbol{\delta\phi}}_-(q) \tag{SI.20}$$

for $m = AB, PH$, where the two modes are $\boldsymbol{\delta\phi}_{AB} = \frac{1}{\sqrt{2}}(1,-1)^\intercal$ and $\boldsymbol{\delta\phi}_{PH} = \frac{1}{\sqrt{f_A^2+f_B^2}}(f_A, f_B)^\intercal$. The affiliated coefficients, $\mathbf{c} := (c_+, c_-)^\intercal$, are given by

$$\mathbf{c}_m = T^{-1}\boldsymbol{\delta\phi}_m \tag{SI.21}$$

where $T = (\boldsymbol{\delta\phi}_+, \boldsymbol{\delta\phi}_-)^\intercal$ is the transformation matrix from the basis of eigenvectors into the Cartesian coordinates. Since the modes *AB* and *PH* are no eigenvectors, a system initialized with these will also excite other modes. Hence, to gain an insight into their contribution to the above growth rates, we need to look at the instantaneous, or short time behavior, when other modes are not yet excited and project onto the respective modes. This yields

$$\mathfrak{P}_m(q,t) := \boldsymbol{\delta\phi}_m \cdot \boldsymbol{\delta\phi}(q,t) = c_{+,m}(q)\left(\boldsymbol{\delta\phi}_m \cdot \boldsymbol{\delta\phi}_+(q)\right)e^{\sigma_+(q)t} + c_{-,m}(q)\left(\boldsymbol{\delta\phi}_m \cdot \boldsymbol{\delta\phi}_-(q)\right)e^{\sigma_-(q)t} \tag{SI.22}$$

which denotes the growth of the amplitude of mode $\boldsymbol{\delta\phi}_m$ independent of excitation of other modes, with $\mathfrak{P}(q,0) = 1\,\forall q$.

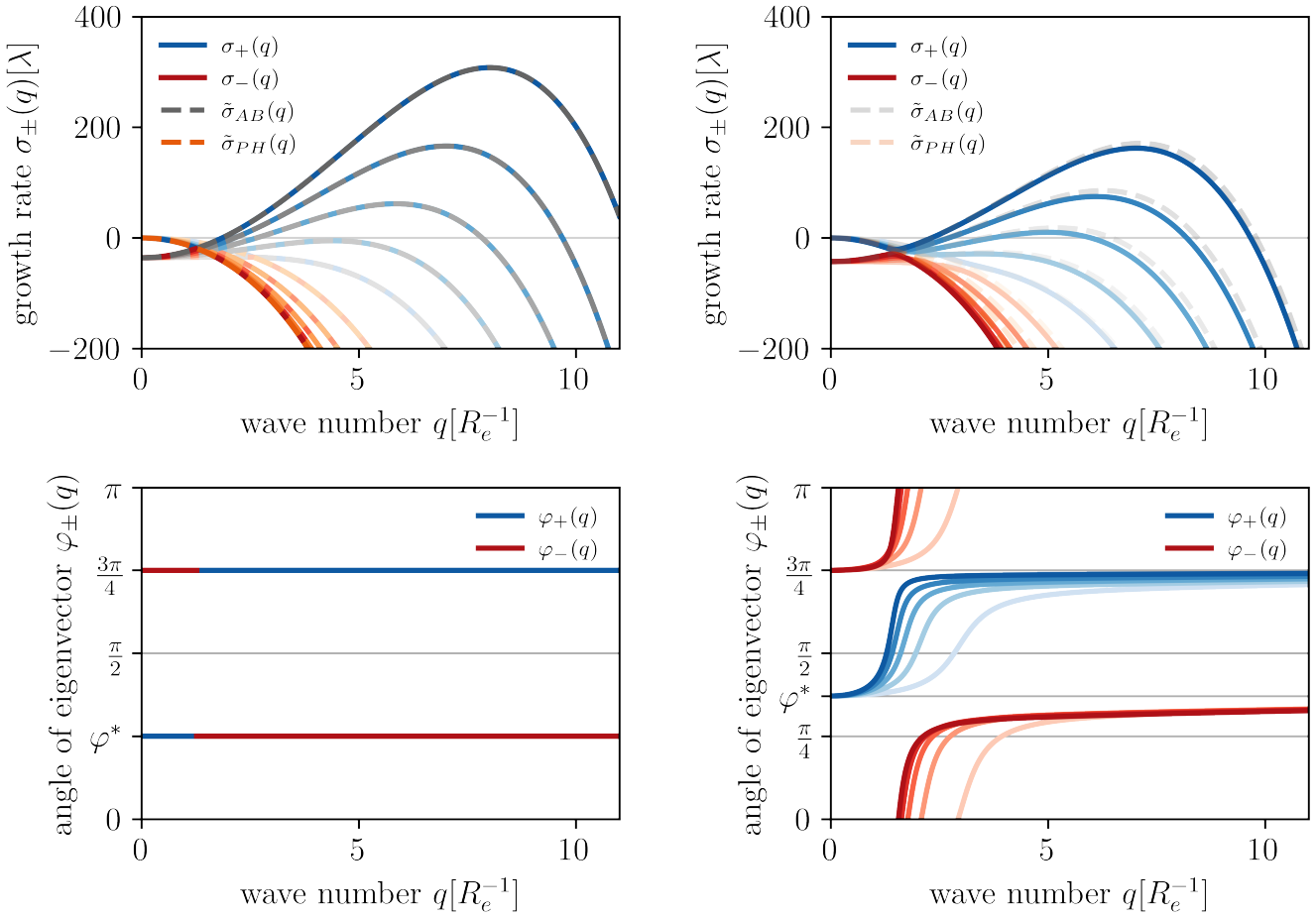

Fig. SI.1 Growth rates $\sigma_\pm(q)$ (top) and corresponding eigenvector angles $\varphi(q)$ (bottom) plotted against the wavevector q for symmetric ($f_A = 0.5$, left) and asymmetric ($f_A = 0.3$, right) diblock copolymers (amphiphiles) in a nonselective solvent for various mean polymer concentrations (lighter shades correspond to lower ρ_P in steps of $\Delta\rho_P = 0.2$, starting at $\rho_P = 0.2$. Flory-Huggins parameters are $\chi_{AB} = 3$, $\chi_{AH} = 0$, $\chi_{BH} = 0$.

From this one can obtain the projected growth rate of mode $m = AB, PH$ as the time derivative of its logarithm,

$$\tilde{\sigma}_m := \frac{\mathrm{d}}{\mathrm{d}t} \ln \mathfrak{P}_m(q,t)\Big|_{t=0} \tag{SI.23}$$

$$= c_{+,m}(q)\left(\boldsymbol{\delta\phi}_m \cdot \boldsymbol{\delta\phi}_+(q)\right)\sigma_+(q) + c_{-,m}(q)\left(\boldsymbol{\delta\phi}_m \cdot \boldsymbol{\delta\phi}_-(q)\right)\sigma_-(q) \tag{SI.24}$$

which denotes the growth rate contribution of the modes m to those of the eigenvectors and are shown in Figure SI.1 as dashed lines.

For asymmetric copolymers in nonselective solvent, the growth eigenmodes correspond to the *PH* and *AB* process as follows. For small qR_e the fastest growing mode resembles the macrophase-separation process *PH*, whereas for large qR_e the fastest growing mode has more the character of microphase separation *AB*. For larger qR_e, the slower mode resembles the *PH* process but it is suppressed, $\sigma_- < 0$, corresponding to a decay of composition fluctuations (mixing) between amphiphilic product and hydrophphilic components. The angle, φ_-, however, remains smaller than φ^*, *i. e.*, $\delta\phi_B/f_B < \delta\phi_A/f_A$, indicating an entropic preference of the nonselective solvent towards the minority block, *A*.

For the situation of repulsive solvent, where the homogeneous solution becomes unstable to both processes at different wave numbers, one can observe a double peak structure in the larger growth rate, as shown in Figure SI.2. Here it becomes additionally visible that the growth rate is the results of two unstable modes with overlapping peaks.

In a more general case, however, the two peaks are wider and can overlap in such a way that only one peak is visible in the larger eigenvalue, $\sigma_+(q)$. This is the case especially, when the polymer-solvent segregation becomes stronger and its

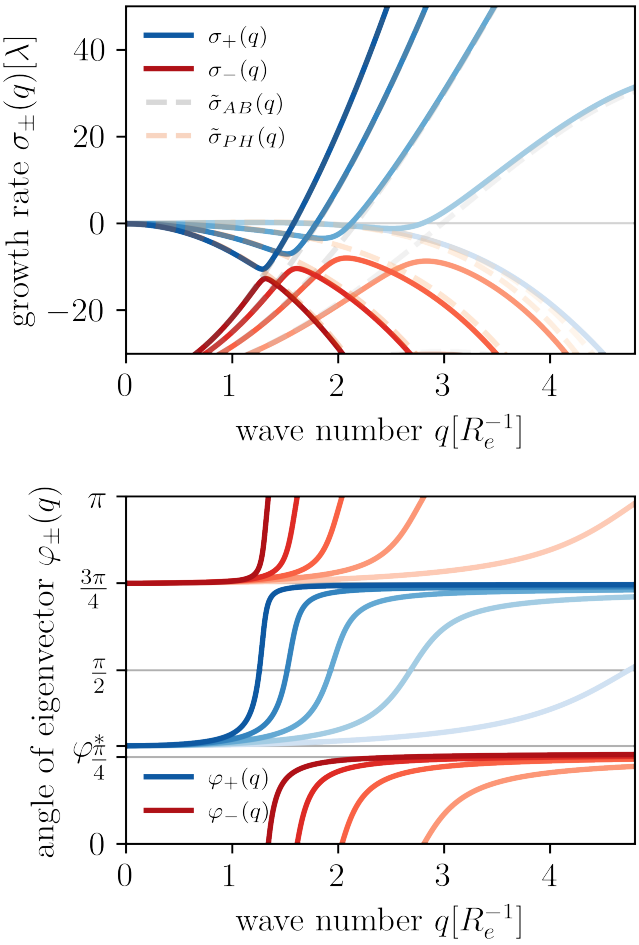

Fig. SI.2 Growth rates $\sigma_\pm(q)$ (top) and corresponding eigenvector angles $\varphi_\pm(q)$ plotted against the wavevector q for a slightly asymmetric diblock copolymer, $f_A = 0.45$, in an incompatible solvent for various polymer mean concentration, colored as in Figure SI.1. Flory-Huggins parameters are $\chi_{AB} = 4$, $\chi_{AH} = 2$, $\chi_{BH} = 2$. The growth-rate of the *PH* and *AB* processes are given as dashed and dotted lines as computed in Equation SI.24.

corresponding peak widens. The above projection method still allows to observe the respective contribution of the *PH* and *AB* process. This is the case, if we consider the system of the main text, an asymmetric, amphiphilic diblock copolymer in aqueous solution, *i. e.*, where the majority block has a strong repulsion toward the solvent. The result is shown in Figure SI.3. One can observe that, starting from homogeneous solution with low polymer concentration, the block-block segregation is not immediately growing. Rather the segregation will start once the polymer has phase-separated from the solvent. A stronger block-block interaction will change this behavior and actually result in the block-block segregation being the faster growing process, even at low polymer concentrations, as demonstrated on the right in Figure SI.3.

Reactions in the system will shift the above growth rate downwards, independent of the wave number, q. While this will transforms the macrophase separating process *PH* to become microphase separating, as the smallest wave numbers are suppressed, the change of initial growth of fluctuations from the homogeneous solution is small for strongly segregated systems. Rather, the effects of an effective microphase separation in the *PH* process will become dominant in the long-time limit which can be treated by mapping the system onto known equilibrium dynamics. This is done in the following section.

3 Effective Free-Energy Functional

The linear stability analysis of the previous section determines the short-time evolution. Here we will show that the nonequilibrium stationary state formed by Reaction-Driven Assembly (RDA) consists of a dense lattice of aggregates. To this end, we demonstrate that the ordering phenomena can be approximately mapped onto the ordering kinetics of an equivalent diblock copolymer melt described by an equilibrium free-energy functional, *i. e.*, the evolution equations for (i) homogeneous fuel concentration and (ii) joint distribution of hydrophilic components, *S* and *R*, can be written as potential

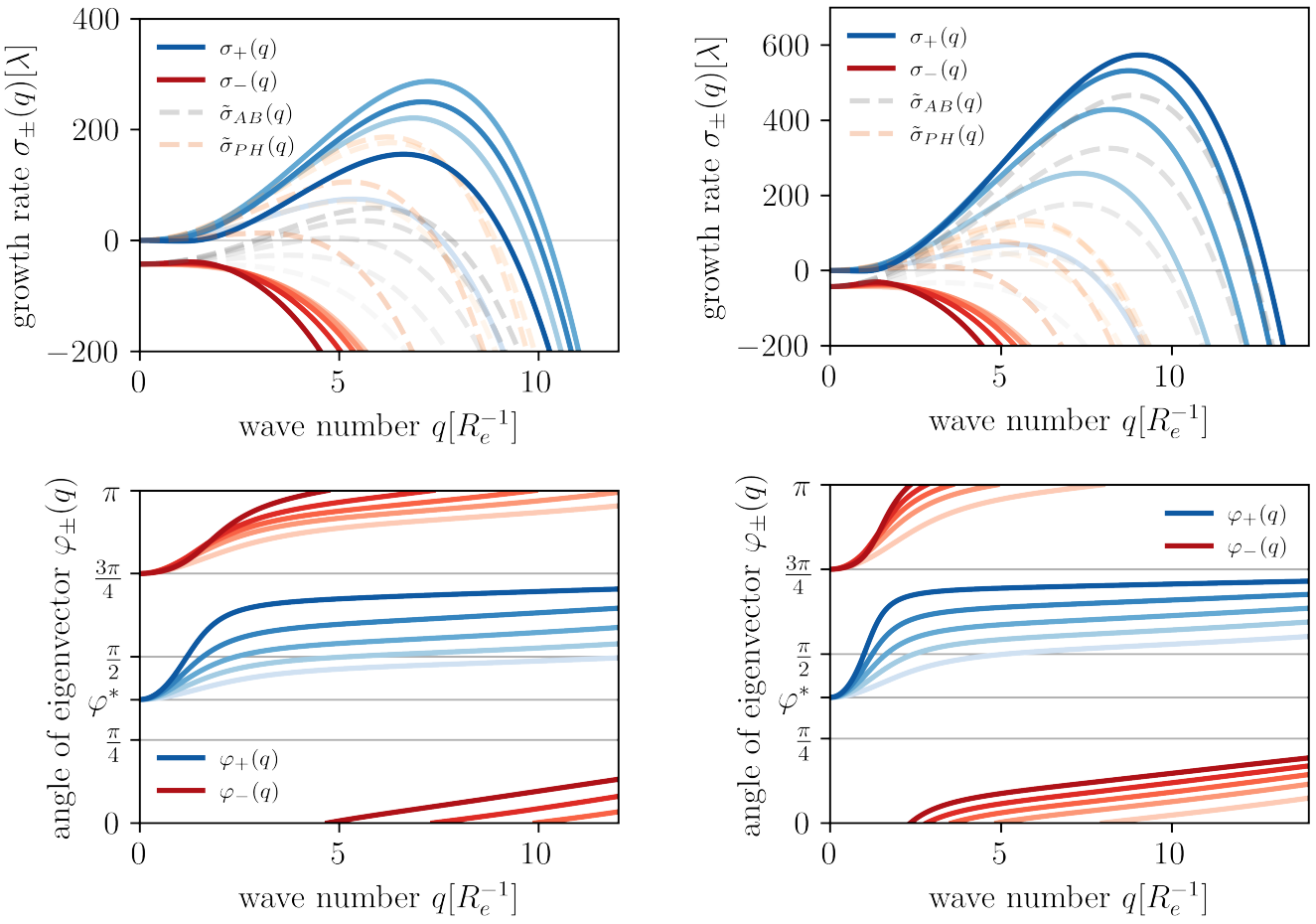

Fig. SI.3 Growth rates $\sigma_\pm(q)$ and projected growth rates $\tilde{\sigma}_{AB/PH}$ (top) and corresponding eigenvector angles $\varphi(q)$ plotted against the wave number q for an asymmetric, amphiphilic diblock copolymer, $f_A = 0.3$, $\chi_{AH} = 0.5$, $\chi_{BH} = 4$, in aqueous solution for various polymer mean concentrations, colored as in Figure SI.1. The block-block repulsion taken in the main text, $\chi_{AB}N_P = 20$ is shown on the left, while a stronger one, $\chi_{AB}N_P = 40$ is shown on the right.

dynamics in an effective free-energy landscape that is equivalent to one of block copolymers.

Initially, we do so for a simplified system, where we replace the amphiphilic product by hydrophobic homopolymer P, *i. e.*, $f_A = 0$. Thus, we study an incompressible binary mixture of hydrophobic product, P, and hydrophilic species, H – solvent and precursor/reactant. Afterwards we generalize our result to an amphiphilic product.

To understand the effect of RDA, we write down the evolution equation for the product polymer P,

$$\frac{\partial \phi_P}{\partial t} = \frac{\lambda R_e^5}{\sqrt{\mathcal{N}} k_B T} \nabla \cdot (\phi_P \nabla \mu_P) + r_f N_P \rho_F \rho_R / \rho_H \phi_H - r_b N_P \phi_P \tag{SI.25}$$

$$= \frac{\lambda R_e^5}{\sqrt{\mathcal{N}} k_B T} \nabla \cdot (\phi_P \nabla \mu_P) + \underbrace{r_f N_P \rho_F \rho_R - r_b N_P \rho_P}_{\text{stationarity}=0}$$

$$+ \frac{r_f N_P \rho_F \rho_R}{\rho_H} (\phi_H - \rho_H) - r_b N_P (\phi_P - \rho_P) \tag{SI.26}$$

where we have again split the densities into a spatially homogeneous part, ρ_c, and the deviations from it, $\delta\phi_c = \phi_c - \rho_c$. Starting from arbitrary mean concentration ρ_i, these will exponentially fast approach the stationary ones,

$$r_b \rho_P = r_f \rho_F \rho_R \tag{SI.27}$$

such that the terms that only contain spatial averages cancel. Then, the time evolution can be approximated in an effective form to recover complete model-B dynamics, *i. e.*

$$\frac{\partial \phi_P}{\partial t} = \lambda R_\mathrm{e}^2 \nabla \cdot \Bigg[\phi_P \nabla \Bigg\{ \frac{R_\mathrm{e}^3 \mu_P(\mathbf{r})}{\sqrt{\mathscr{N}} k_\mathrm{B} T} - \int \frac{\mathrm{d}\mathbf{r}'}{R_\mathrm{e}^3} \frac{R_\mathrm{e} \mathscr{G}(\mathbf{r}-\mathbf{r}')}{\lambda \rho_P} \left(\frac{r_f N_P \rho_F \rho_R}{\rho_H} \delta\phi_H(\mathbf{r}') - r_b N_P \delta\phi_P(\mathbf{r}') \right) \Bigg\} \Bigg] + \mathscr{O}(\delta\phi_c^2) \tag{SI.28}$$

$$= \frac{\lambda R_\mathrm{e}^5}{\sqrt{\mathscr{N}} k_\mathrm{B} T} \nabla \cdot \left[\phi_P \nabla \mu_P^\mathrm{eff} \right] + \mathscr{O}(\delta\phi_c^2) \tag{SI.29}$$

and likewise for the second, hydrophilic component,

$$\frac{\partial \phi_H}{\partial t} = \lambda R_\mathrm{e}^2 \nabla \cdot \Bigg[\phi_H \nabla \Bigg\{ \frac{R_\mathrm{e}^3 \mu_H(\mathbf{r})}{\sqrt{\mathscr{N}} k_\mathrm{B} T} - \int \frac{\mathrm{d}\mathbf{r}'}{R_\mathrm{e}^3} \frac{R_\mathrm{e} \mathscr{G}(\mathbf{r}-\mathbf{r}')}{\lambda \rho_H} \left(r_b N_P \delta\phi_P(\mathbf{r}') - \frac{r_f N_P \rho_F \rho_R}{\rho_H} \delta\phi_H(\mathbf{r}') \right) \Bigg\} \Bigg] + \mathscr{O}(\delta\phi_c^2) \tag{SI.30}$$

$$= \frac{\lambda R_\mathrm{e}^5}{\sqrt{\mathscr{N}} k_\mathrm{B} T} \nabla \cdot \left(\phi_P \nabla \mu_H^\mathrm{eff} \right) + \mathscr{O}(\delta\phi_c^2) \tag{SI.31}$$

where we introduced effective chemical potentials $\mu_c^\mathrm{eff} = \delta \mathscr{F}^\mathrm{eff} / \delta \phi_c$ that can be derived from an effective free-energy functional

$$\frac{\mathscr{F}^\mathrm{eff}[\{\phi_c\}]}{\sqrt{\mathscr{N}} k_\mathrm{B} T} = \frac{\mathscr{F}[\{\phi_c\}]}{\sqrt{\mathscr{N}} k_\mathrm{B} T} + \mathscr{O}(\delta\phi_c^3) + \frac{r_b N_P \rho_P}{2\lambda} \iint \frac{\mathrm{d}\mathbf{r}}{R_\mathrm{e}^3} \frac{\mathrm{d}\mathbf{r}'}{R_\mathrm{e}^3} \left[\frac{\delta\phi_P(\mathbf{r})}{\rho_P} - \frac{\delta\phi_H(\mathbf{r})}{\rho_H} \right] R_\mathrm{e} \mathscr{G}(\mathbf{r}-\mathbf{r}') \left[\frac{\delta\phi_P(\mathbf{r}')}{\rho_P} - \frac{\delta\phi_H(\mathbf{r}')}{\rho_H} \right], \tag{SI.32}$$

where we have used Equation SI.27. Also note that $\delta\phi_H/\rho_H = \delta\phi_R/\rho_R$ because of assumption (ii). Therefore, the constant turnover of precursor to product and *vice versa* introduces an effective term to the free energy that corresponds to a weak connectivity between the two chemically active components, R and P, in agreement with similar work[58,60]

A similar argument can be made for the RDA of amphiphiles. Again, we consider simplification (i) and (ii), and this time treat ϕ_A and ϕ_B separately. This procedure yields the effective free-energy functional

$$\frac{\mathscr{F}^\mathrm{eff}[\{\phi_c\}]}{\sqrt{\mathscr{N}} k_\mathrm{B} T} = \frac{\mathscr{F}[\{\phi_c\}]}{\sqrt{\mathscr{N}} k_\mathrm{B} T} + \frac{r_b N_P \rho_P}{2\lambda} \iint \frac{\mathrm{d}\mathbf{r}}{R_\mathrm{e}^3} \frac{\mathrm{d}\mathbf{r}'}{R_\mathrm{e}^3} R_\mathrm{e} \mathscr{G}(\mathbf{r}-\mathbf{r}') \times \Bigg[f_A \frac{\delta\phi_A(\mathbf{r}) \delta\phi_A(\mathbf{r}')}{\rho_A \rho_A} + f_B \frac{\delta\phi_B(\mathbf{r}) \delta\phi_B(\mathbf{r}')}{\rho_B \rho_B} - 2 \frac{\delta\phi_H(\mathbf{r}) \{ \delta\phi_A(\mathbf{r}') + \delta\phi_B(\mathbf{r}') \}}{\rho_H \{\rho_A + \rho_B\}} + \frac{\delta\phi_H(\mathbf{r}) \delta\phi_H(\mathbf{r}')}{\rho_H^2} \Bigg] + \mathscr{O}(\delta\phi_c^3), \tag{SI.33}$$

where $\rho_P = \rho_A/f_A = \rho_B/f_B$. Again, in the nonequilibrium steady state, the reactions give rise to an effective, weak connectivity between hydrophilic precursor and the blocks of the amphiphilic diblock copolymer, which scales with the reaction rate.

We can obtain the corresponding inverse structure factor of the homogeneous state as the second-order vertex function in the above free-energy expansion, *i. e.*, the Hessian of the free energy with respect to the concentration fields. This is most easily done in Fourier space

$$\mathscr{S}_{cc'}^{-1}(\mathbf{q}) = \frac{\partial^2 \mathscr{F}^\mathrm{eff}[\phi_A(\mathbf{q}'), \phi_B(\mathbf{q}'), \phi_H(\mathbf{q}')]}{\partial \phi_c(\mathbf{q}) \partial \phi_{c'}(\mathbf{q})} = \frac{\partial \mu_c^\mathrm{eff}(\mathbf{q})}{\partial \phi_{c'}(\mathbf{q})} \tag{SI.34}$$

for $c,c' = A,B,H$. By virtue of incompressibility, we replace $\phi_H(\mathbf{q}) = 1-\phi_A(\mathbf{q})-\phi_B(\mathbf{q})$, omitting the Lagrange field, π. This way, the curvature of the free energy becomes a 2×2-matrix, with

$$\mathscr{S}^{-1}_{cc'}(\mathbf{q}) = \frac{\partial^2 \mathscr{F}^{\text{eff}}[\phi_A(\mathbf{q}'),\phi_B(\mathbf{q}'),1-\phi_A(\mathbf{q}')-\phi_B(\mathbf{q}')]}{\partial\phi_c(\mathbf{q})\partial\phi_{c'}(\mathbf{q})} = \frac{\partial\mu^{\text{eff}}_c(\mathbf{q})}{\partial\phi_{c'}(\mathbf{q})} - \frac{\partial\mu^{\text{eff}}_H(\mathbf{q})}{\partial\phi_{c'}(\mathbf{q})} \tag{SI.35}$$

for now $c,c' = A,B$. We can relate this quantity to the linearized evolution operator of the previous section, $\hat{\Sigma}(q)$. For this, we notice that the incompressible model-B dynamics of Equation SI.11 can be written as

$$\frac{\partial\phi_c(\mathbf{r})}{\partial t} = \nabla\cdot\left[\sum_{c'}\Lambda_{cc'}\nabla(\mu^{\text{eff}}_{c'}(\mathbf{r})-\mu^{\text{eff}}_H(\mathbf{r}))\right] \tag{SI.36}$$

with the nondiagonal Onsager matrix

$$\Lambda_{cc'}(\mathbf{r}) = \frac{\lambda R_e^5}{\sqrt{\mathscr{N}}k_BT}\begin{pmatrix} \phi_A(\mathbf{r})\phi_B(\mathbf{r})+\phi_A(\mathbf{r})\phi_H(\mathbf{r}) & -\phi_A(\mathbf{r})\phi_B(\mathbf{r}) \\ -\phi_A(\mathbf{r})\phi_B(\mathbf{r}) & \phi_A(\mathbf{r})\phi_B(\mathbf{r})+\phi_B(\mathbf{r})\phi_H(\mathbf{r}) \end{pmatrix}. \tag{SI.37}$$

Linearizing Equation SI.36 and Fourier transforming, we obtain up to $\mathscr{O}(\delta\phi_c^2)$

$$\frac{\partial\phi_c(\mathbf{q})}{\partial t} = -\mathbf{q}^2\sum_{c',\tilde{c}}\tilde{\Lambda}_{cc'}\underbrace{\left(\frac{\partial\mu^{\text{eff}}_{c'}}{\partial\phi_{\tilde{c}}(\mathbf{q})}-\frac{\partial\mu^{\text{eff}}_H}{\partial\phi_{\tilde{c}}(\mathbf{q})}\right)}_{=\mathscr{S}^{-1}_{c'\tilde{c}}}\phi_{\tilde{c}}(\mathbf{q}) = \hat{\Sigma}_{c\tilde{c}}(\mathbf{q})\phi_{\tilde{c}}(\mathbf{q}) \tag{SI.38}$$

with the constant Onsager matrix

$$\tilde{\Lambda}_{cc'} = \frac{\lambda R_e^5}{\sqrt{\mathscr{N}}k_BT}\begin{pmatrix} \rho_A\rho_B+\rho_A\rho_H & -\rho_A\rho_B \\ -\rho_A\rho_B & \rho_A\rho_B+\rho_B\rho_H \end{pmatrix}. \tag{SI.39}$$

Thus the curvature of the free energy can be written in terms of the linearized evolution operator as

$$\mathscr{S}^{-1}(\mathbf{q}) = -\tilde{\Lambda}^{-1}\frac{\hat{\Sigma}(\mathbf{q})}{\mathbf{q}^2} \tag{SI.40}$$

The homogeneous solution becomes unstable if $\mathscr{S}^{-1}(\mathbf{q})$ possesses a negative eigenvalue. Similar to the linearized evolution operator, $\hat{\Sigma}(\mathbf{q})$, in general, the eigenmodes of $\mathscr{S}^{-1}(\mathbf{q})$ do not directly correspond to the demixing processes *PH* or *AB*, but are a linear combination of these. However, as before, we can project onto the respective process modes and gain insights into their contributions to the eigenmodes. This change of the projections of the inverse structure factor with reaction rates is presented in the left-hand side plots of Figure 2 and discussed in the main text.

4 Numerical Implementation

We use a pseudo-spectral method to numerically propagate the system of coupled partial differential equations, employing a Fast Fourier Transformation (FFT) combined with semi-implicit Euler time-stepping. A major problem for the numerical stability is the divergence of the chemical potentials for small densities, $\mu_c \overset{\phi_c\to 0}{\longrightarrow} -\infty$. It proves to be numerically stabilizing to use an auxiliary order-parameter field, $\psi(\mathbf{r},t) = \sqrt{\phi(\mathbf{r},t)}$, for which the corresponding chemical potential $\tilde{\mu}_c(\mathbf{r}) = \delta\mathscr{F}/\delta\psi_c(\mathbf{r}) = 2\psi_c(\mathbf{r})\mu_c(\mathbf{r})$ vanishes for small densities[48]. In doing so, the density-conserving part of Equation SI.4-SI.7 without thermal noise can be rewritten to

$$\frac{\partial\phi_c}{\partial t}\frac{\sqrt{\mathscr{N}}k_BT}{\lambda R_e^5} = \nabla\cdot[\phi_c\nabla\mu_c] = \nabla\cdot\left[\psi_c^2\nabla\frac{\tilde{\mu}_c}{2\psi_c}\right] \tag{SI.41}$$

$$= \frac{1}{2}\nabla\cdot[\psi_c\nabla\tilde{\mu}_c-\tilde{\mu}_c\nabla\psi_c] = \frac{1}{2}\left[\psi_c\nabla^2\tilde{\mu}_c-\tilde{\mu}_c\nabla^2\psi_c\right] \tag{SI.42}$$

In this representation, all quantities are well-behaved and the Laplacians ∇^2 can be readily evaluated in Fourier space.

Given a morphology $\{\phi_c(\mathrm{r},t)\}$ and temporal discretization Δt, one (i) calculates the chemical potentials and (ii) generates the spatially correlated, random fields that fulfill the fluctuation-dissipation relation, Equation 10. This is done from

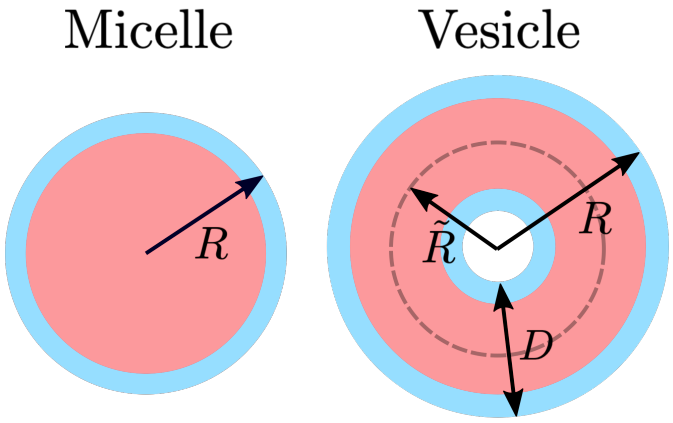

Fig. SI.4 Measured radii for the spherical micelles and vesicles. The radius R is always measured to the outer border, while $\tilde{R}$ measures to center of the vesicle's bilayer of thickness D.

spatially and temporally uncorrelated Gaussian random fields with unit variance, as described in Ref.[48]. Having these one wishes to obtain the density fields at time $t+\Delta t$. Note that the Laplacian of the chemical potential contains a term proportional to $-\nabla^4\phi_c$. In Fourier space this becomes $-\mathbf{q}^4\hat{\phi}_c$ for wavevector $\mathbf{q}$ and Fourier transformed $\hat{\phi}_c$. High Fourier modes are thus highly damped, however, treating such a term explicitly will necessitate minuscule time steps. Hence these are treated implicitly. One problem is that these terms in general are not linear in ϕ_c. In principle, it is possible to evaluate these using a finite-differences scheme and solving a set of sparse linear equations for the inversion[50]. Here, we resolve to treating only a single term that is linear in ϕ_c implicitly. Inverting is now trivially done in Fourier space. The final time evolution hence reads

$$(1+\Delta t\lambda\ell_c R_\mathrm{e}^4\nabla^4)\phi_c(\mathbf{r},t+\Delta t)=\phi_c+\Delta t\lambda\ell_c R_\mathrm{e}^4\nabla^4\phi_c+\frac{\Delta t\lambda R_\mathrm{e}^5}{2\sqrt{\mathcal{N}}k_\mathrm{B}T}\left[\psi_c\nabla^2\tilde{\mu}_c-\tilde{\mu}_c\nabla^2\psi_c\right]+\sqrt{\Delta t}\xi_c \tag{SI.43}$$

where $\lambda\ell_c R_\mathrm{e}^4$ is the linear prefactor for each component and all fields on the right hand side (r.h.s.) are evaluated at $(\mathbf{r},t)$. To obtain the time-propagated concentration fields, one needs to (iii) evaluate the r.h.s. and (iv) invert the linear equation in Fourier space, using $\hat{\phi}_c(\mathbf{q},t+\Delta t)=\frac{1}{1+\Delta t\lambda\ell_c(qR_\mathrm{e})^4}[\hat{\text{r.h.s.}}]$. The final step (v) consists of regularizing the concentration fields to keep them positive. Unlike Ref.[48], we cannot simply set the concentration fields to zero, where they become negative because such a procedure does not conserve ρ_c and significantly influences the spatially average concentrations over long times. Instead, we take the material that is necessary to keep the concentration positive from a randomly drawn neighboring cell. Doing so in a parallel fashion requires the use of atomic operations, for reading out the availability of material from the neighbor and subsequently taking it after checking that its value has not been changed with an atomic compare-and-swap operation.

We implemented the numerical procedure in our `C`-software with Graphics Processing Unit (GPU)-acceleration using the Compute Unified Device Architecture by Nvidia® (CUDA). CUDA readily provides all of the above operations, including a fast implementation of the FFTs, which are most compute time consuming. The code is available open source *via* `www.gitlab.com/g.ibbeken/udm`.

5 Measurement of Micelle and Vesicle Radii

For the measurement of the radii R of individual micelles and vesicles, we perform a Hoshen-Koppelman cluster analysis (HKCA)[75,76]. To this end, we take the tail-group concentration, ϕ_B, and determine where it is greater than $\phi_B^\mathrm{thresh}=\frac{1}{2}$. The HKCA then allows us to distinguish individual micelles and vesicles and obtain a map

$$\eta_\alpha(\mathbf{r})=\begin{cases}1 & \text{where } \phi_B>\phi_B^\mathrm{thresh} \text{ in cluster } \alpha\\ 0 & \text{else.}\end{cases} \tag{SI.44}$$

where the index α runs over all clusters. One can calculate for each cluster its volume v_α, center of mass $\mathbf{r}_{\mathrm{cm},\alpha}$, and radius

of gyration, $\tilde{R}_\alpha$, according to

$$v_\alpha = \int \mathrm{d}\mathbf{r}\, \eta_\alpha(\mathbf{r}) \tag{SI.45}$$

$$\mathbf{r}_{\mathrm{cm},\alpha} = \frac{1}{v_\alpha} \int \mathrm{d}\mathbf{r}\, \eta_\alpha(\mathbf{r})\mathbf{r} \tag{SI.46}$$

$$\tilde{R}_\alpha^2 = \frac{1}{v_\alpha} \int \mathrm{d}\mathbf{r}\, \eta_\alpha(\mathbf{r})|\mathbf{r}-\mathbf{r}_{\mathrm{cm},\alpha}|^2. \tag{SI.47}$$

Note that for a large spherical vesicle, $\tilde{R}_\alpha$ is the vesicle's radius up to corrections of order $\mathscr{O}((D/\tilde{R}_\alpha)^2)$, with D being the bilayer thickness. In doing so we evaluate the cluster radii, R_α, by assuming a spherical shape and distinguishing between micelle and vesicles. In both cases, R_α measures the radius to the very outside, *i. e.*,

$$R_\alpha = \begin{cases} \sqrt{\frac{5}{3}}\tilde{R}_\alpha & \text{if } \eta_\alpha(\mathbf{r}_{\mathrm{cm},\alpha}) = 1 \qquad \text{(micelle)} \\ \tilde{R}_\alpha\left(1+\zeta_\alpha - \frac{1}{\zeta_\alpha}\right) + \mathscr{O}((D_\alpha/\tilde{R}_\alpha)^3) & \text{else.} \end{cases} \tag{SI.48}$$

with the definition

$$\zeta_\alpha := \sqrt[3]{\sqrt{1+\left(\frac{3v_\alpha}{16\pi\tilde{R}^3}\right)^2} + \frac{3v_\alpha}{16\pi\tilde{R}^3}} \tag{SI.49}$$

This way the radius, R_α, stays continuous upon transition from micelle to vesicle, *e. g.*, *via* pathway II. This becomes visible in Figure SI.4: A slightly larger aggregate volume forms a vesicle with a small lumen. Measuring this aggregate's radius to the center of the bilayer would result in a discontinuity in the radius.

6 Kinetics of Structure Formation in Particle-Based Simulations

Here we demonstrate the time evolution in the particle-based simulations, corresponding to the continuum simulations presented in the main text in Figure 3. In Figure SI.5 we present the kinetics of RDA for two reaction rates, $r_b = 5.2\cdot 10^{-3}$ and $r_b = 2.1\cdot 10^{-2}$. One can see the real-space morphology of the product-polymer tails, $\phi_B(\mathbf{r},t)$ as well as the structure factor $\mathscr{S}_{BB}(q)$ in reciprocal space.

In the case of smaller reaction rates, the time-evolution progresses exactly as in the continuum model: vesicles form *via* pathway I and coarsening arrests afterwards such that the vesicles obtain finite and uniform size. In the case of high reaction rates, as given here, the lattice spacing is so small that aggregates remain micelles. However, we observe the emergence of non-spherical aggregates, such as cylindrical and disc-like micelles which stay stable for long times. Additionally, for this kind of amphiphiles chosen in the particle-based model, we do not observe pathway II even for slightly smaller reaction rates which is related to the higher block-block repulsion, $\chi_{AB}N_P$. Both of these examples are also provided as videos with the files `particle-based-impl-fuel-rb5.2e-3.mp4` and `particle-based-impl-fuel-rb1.2e-2.mp4`.

7 Precursor Enrichment in RDA Vesicles

As described in the main text, precursor is enriched inside vesicles formed by RDA. The origin of this behavior can be easily analyzed in the particle-based model. To this end, we set up particle-based simulation with a single vesicle with radius $2.37R_\mathrm{e}$ and bilayer thickness $D = 0.85R_\mathrm{e}$ in a spherical domain with a radius of $R_V = 4.25R_\mathrm{e}$. We use the reaction rates $r_f\rho_F = 4.18\cdot 10^{-2}\tau_0^{-1}$, $r_b = 1.05\cdot 10^{-3}\tau_0^{-1}$, with $\rho_R+\rho_P = 0.25$ and implicitly treat the fuel. In the nonequilibrium stationary state, we track the positions of the individual polymers and categorize them according to (i) being in the precursor/reactant or product state and (ii) whether they are positioned in the inner leaflet/the inside of the vesicles membrane or not. We categorize the polymers in the 4 states every 500MCS $\approx \frac{\tau_0}{5}$ and determine the transition rates between these states. We map the dynamics of polymer states onto a Markov jump process, describing the state occupations by a vector,

$$\boldsymbol{\gamma} = \begin{pmatrix} \mathscr{P}(\text{precursor outside}) \\ \mathscr{P}(\text{precursor inside}) \\ \mathscr{P}(\text{product outside}) \\ \mathscr{P}(\text{product inside}) \end{pmatrix} \tag{SI.50}$$

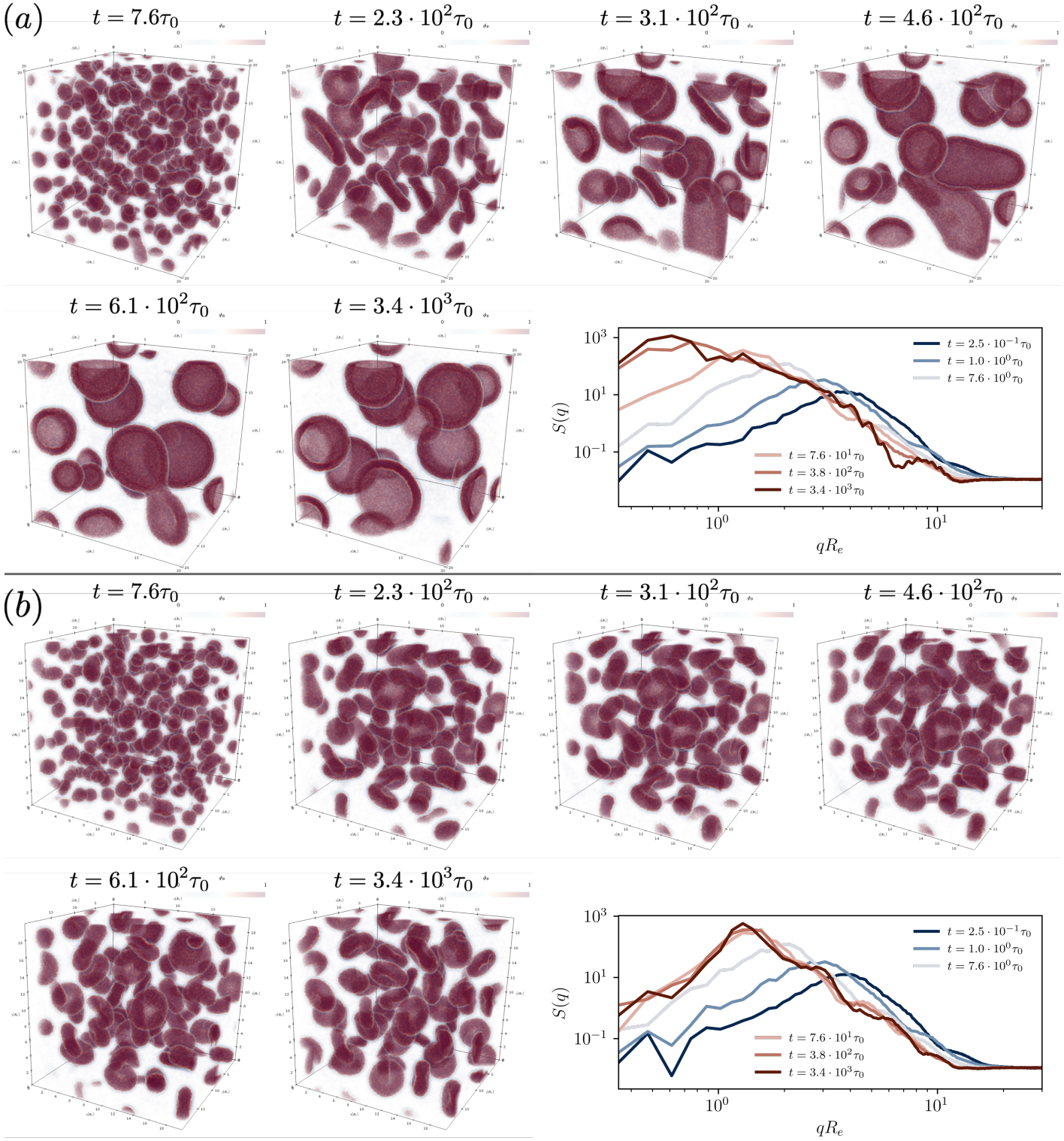

Fig. SI.5 Time evolution of the hydrophobic tail densities in the particle-based simulations starting from a homogeneous initial configuration, both, in real space, $\phi_B(\mathbf{r})$, and in reciprocal q-space, $\mathscr{S}_{BB}(q)$. Reaction rates are chosen (a) $r_f\rho_F = 5.2\cdot10^{-3}\tau_0^{-1}$, $r_b = 1.3\cdot10^{-3}\tau_0^{-1}$ and (b) $r_f\rho_F = 2.1\cdot10^{-2}\tau_0^{-1}$, $r_b = 5.2\cdot10^{-3}\tau_0^{-1}$.

where $\mathscr{P}(\cdot)$ denotes the probability to find a polymer in a certain state. The time evolution of the occupation vector follows

$$\partial_t \boldsymbol{\gamma} = \hat{\mathscr{M}} \boldsymbol{\gamma} \tag{SI.51}$$

and we measured the generator, $\hat{\mathscr{M}}$, *i. e.*, all transition rates

$$\hat{\mathscr{M}} = \begin{pmatrix} -4.29 \cdot 10^{-2} & 5.23 \cdot 10^{-3} & 1.12 \cdot 10^{-2} & 1.05 \cdot 10^{-4} \\ 3.58 \cdot 10^{-3} & -5.39 \cdot 10^{-2} & 9.13 \cdot 10^{-5} & 8.27 \cdot 10^{-3} \\ 3.71 \cdot 10^{-2} & 5.86 \cdot 10^{-3} & -2.98 \cdot 10^{-1} & 7.77 \cdot 10^{-1} \\ 2.11 \cdot 10^{-3} & 4.29 \cdot 10^{-2} & 2.85 \cdot 10^{-1} & -7.87 \cdot 10^{-1} \end{pmatrix} \cdot \tau_0^{-1} \tag{SI.52}$$

The transition rates that explain the precursor enrichment are highlighted. Most notably, in the red box, precursor that is located inside the vesicle originated as amphiphilic product in the inner leaflet of the bilayer membrane and *vice versa*. The blue boxes indicate the slow exchange of precursor across the vesicle's membrane compared to the flip-flopping of product polymers inside the bilayer, displayed in the bottom right quadrant. Finally, the stationary state of this jump process is

$$\lim_{t\to\infty} \boldsymbol{\gamma}(t) = \begin{pmatrix} 0.157 \\ 0.043 \\ 0.583 \\ 0.217 \end{pmatrix} \tag{SI.53}$$

From this one can infer that the precursor density on the outside, $\phi_{R,\text{out}} = \gamma_0 \frac{(\rho_R+\rho_P)V}{V_\text{out}} = \gamma_0(\rho_R+\rho_P)\frac{R_V^3}{R_V^3-R^3} \approx 0.05$, is significantly smaller than on the inside, $\phi_{R,\text{in}} = \gamma_1 \frac{(\rho_R+\rho_P)V}{V_\text{in}} = \gamma_1(\rho_R+\rho_P)\frac{R_V^3}{(R-D)^3} \approx 0.245$. Furthermore the fraction of precursor polymers on the inside $\gamma_1/(\gamma_0+\gamma_1) \approx 0.22$ is only slightly lower than the fraction of product polymers on the inner leaflet of the bilayer $\gamma_3/(\gamma_2+\gamma_3) \approx 0.27$.